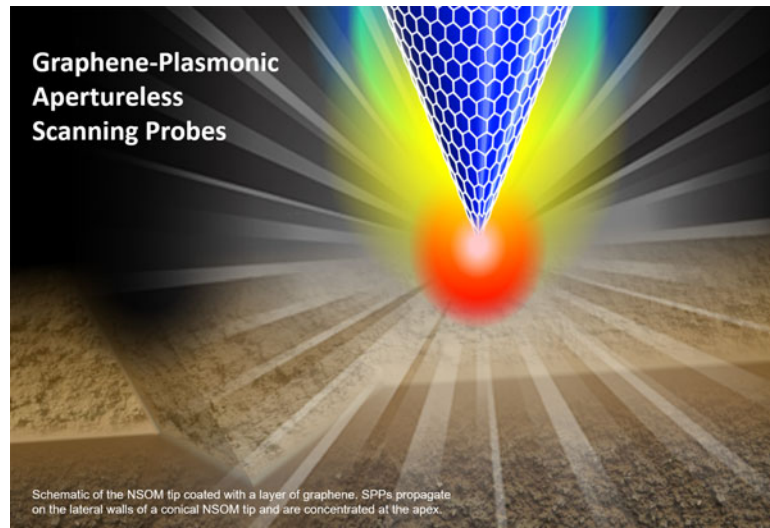


Apertureless Near-Field Scanning Probes Based on Graphene Plasmonics

Volume 9, Number 1, February 2017

Hamid T. Chorsi, *Student Member, IEEE*

John X. J. Zhang, *Senior Member, IEEE*



DOI: 10.1109/JPHOT.2017.2657322

1943-0655 © 2017 IEEE

Apertureless Near-Field Scanning Probes Based on Graphene Plasmonics

Hamid T. Chorsi, *Student Member, IEEE*,
and John X. J. Zhang, *Senior Member, IEEE*

Thayer School of Engineering, Dartmouth College, Hanover, NH 03755 USA

DOI:10.1109/JPHOT.2017.2657322

1943-0655 © 2017 IEEE. Translations and content mining are permitted for academic research only.
Personal use is also permitted, but republication/redistribution requires IEEE permission.
See http://www.ieee.org/publications_standards/publications/rights/index.html for more information.

Manuscript received December 5, 2016; revised January 18, 2017; accepted January 19, 2017. Date of publication January 25, 2017; date of current version February 9, 2017. This work was supported in part by the National Institute of Health (NIH Director's Transformative Research Award R01HL137157), by the National Science Foundation (NSF CAREER Award Grant 0846313), and by the Defense Advanced Research Projects Agency Young Faculty Award N66001-10-1-4049. Corresponding author: J. X. J. Zhang (e-mail: john.zhang@dartmouth.edu).

Abstract: We present a novel approach in designing high-throughput high-resolution apertureless near-field scanning probes with enhanced nanofocusing based on graphene plasmonics. Extremely localized plasmons on graphene are mingled with nanofocusing of surface plasmon polaritons to confine and steer the plasmon waves into the apex of a near-field scanning optical microscopy tip. The Fermi level, localized emission sites on graphene, and the angle of excitation play a critical role in exciting graphene surface plasmons on the lateral walls of the designed conical probes. The optimized probes feature full-width at half-maximum (FWHM) around 25 nm, which is at least two times smaller than conventional metallic plasmonic tips. The near-field electromagnetic properties of the designed probes are characterized in detail and compared to the conventional single-aperture and typical apertureless metallic plasmonic (silver and gold) probes. Over three orders of magnitude electric field enhancement compared to metallic probes on SiO₂ substrate has been achieved.

Index Terms: Plasmonics, nanostructures, microscopy, fabrication and characterization.

1. Introduction

Plasmonic nanofocusing (PNF) aims to localize optical energy at the nanoscale by using surface plasmon waves, which are collective oscillations of conduction electrons excited via polarized light at the interface between a negative and positive permittivity material [1]. Due to their evanescent nature, surface plasmons can manipulate the optical energy of light by concentrating the optical radiation into hot spots with dimensions well below the excitation wavelength. Recently, PNF has been extensively investigated for a variety of applications, including biosensing and nano-sensing [2], subwavelength ultra-high spatial resolution (axial resolution and lateral resolution) optical imaging [3], nanoscale light sources, quantum optics, and tip-enhanced Raman spectroscopy [3]–[5]. In particular, near-field scanning optical microscopy (NSOM) with PNF has recently emerged as a propitious tool for light energy compression to the nanoscale [6]. NSOM is a powerful and unique tool for measurements with a high spatial, energy, and momentum resolution and can be exploited in a variety of applications ranging from nanofabrication to bio-imaging. Noble metal plasmonics (mainly silver and gold) has been at the center of attention in PNF due to the abundance of free electrons which results in a negative real permittivity at visible wavelength range. Surface

plasmon polaritons (SPPs) on metals such as gold and silver suffer from substantial losses, including carrier scattering damping and carrier transitions (interband transitions) in optical frequencies. Besides, metallic plasmonics manifest weak field confinement at THz frequencies mainly because the frequencies are far away from that of the bulk plasmon oscillation of metals [7]. The losses are detrimental to the performance of plasmonic devices and seriously limit their feasibility in metallic plasmonic applications. Aside from the loss issue, some metallic plasmonic material such as silver is not suitable for real plasmonic applications due to their high oxidation susceptibility. There are other issues associated with metallic plasmonics such as fabrication and integration which seriously degrade their applicability and functionality in future applications in optoelectronics and biosensors.

Graphene, a planar sheet of sp^2 -hybridized carbon atoms coordinated in a 2-D hexagonal lattice, is a new vanguard in photonics and optoelectronics [8], [9]. The unique and superior electrical and optical properties of graphene make it an ideal candidate for manipulating the flow of an electromagnetic wave at the nanoscale. Since its first isolation in 2004 [10], extensive research has been done on graphene. Recently, it has been shown both theoretically and experimentally that graphene supports the propagation of SPPs at the interface [11]. Graphene plasmons have lower loss than Noble metal plasmons and display very strong lateral confinement due to shorter excitation wavelength of plasmon oscillations. Besides, graphene plasmon resonances can be tuned owing to its relativistic-like linear energy dispersion (Dirac cone). Charge carriers can be induced through chemical doping or electrostatic gating in the terahertz and infrared region. These characteristics make graphene a suitable choice to be used on curved and bended surfaces.

In this study, we present a novel approach to design apertureless NSOM probes with enhanced near-field and high optical power throughput. Particularly, we combine graphene plasmonics on the lateral side walls of the tip with nanofocusing of SPPs through adiabatic propagation towards an apertureless tip. In this work two NSOM probes have been considered. Structure one (type A) consists of a SiO_2 tip with permittivity $\epsilon_{\text{SiO}_2} = 2.1638$ at 960 nm (312 THz) and a layer of graphene on the lateral surfaces. The second structure (type B) includes an extra layer of low refractive index dielectric on top of SiO_2 tip to provide stronger field confinement.

2. Simulation Results and Discussion

The key factors to excite plasmon waves on graphene at this wavelength of operation is high doping (Fermi) level and appropriate angle of excitation. Optimal design parameters including optical and electrical properties of graphene and dimensions are obtained via a 2-D finite element method (FEM) solver in COMSOL. A conceptual schematic of the device is shown in Fig. 1.

Here, graphene is modeled as a thin layer with a thickness of 0.34 nm, as the graphene layers are separated by ~0.34 nm in graphite. The conductivity profile of graphene is calculated based on the Kubo formula as in (1), shown below [12], [13]. The conductivity parameters are, the momentum relaxation time of $\tau = 0.1$ ps, chemical potential (Fermi velocity, E_F) of $\mu_c = 1$ eV and temperature $T = 300$ K.

$$\sigma_{\text{graphene}}(\omega) = \sigma_{\text{intra}}(\omega) + \sigma_{\text{inter}}(\omega) = \frac{2ie^2T}{\pi\hbar(\omega + i\tau^{-1})} \ln \left[2 \cosh \left(\frac{\mu_c}{2T} \right) \right] \\ + \frac{e^2}{4\hbar} \left[\theta(\omega - 2\mu_c) - \frac{i}{2\pi} \ln \frac{(\omega + 2\mu_c)^2}{(\omega - \mu_c)^2} \right] \quad (1)$$

where e is the electron charge, \hbar is the reduced Plank's constant, ω is the radian frequency, and $\theta(\omega - 2\mu_c)$ denotes a step function. The first term in (1) (Drude-like form) describes the intraband carrier relaxation contribution, and the second term describes the interband carrier transition contribution. As it can be seen from (1), the propagation of SPPs on graphene is largely dependent on the Fermi level. Fig. 2 shows the calculated permittivity of graphene for different values of the Fermi level at the frequency range of 100 THz to 400 THz. Note that $\text{Re}(\epsilon_g)$ approaches the free space permittivity at higher frequencies due to saturation of the graphene conductivity to its universal value $\pi e^2/(2h)$ [14], [15]. Furthermore, the imaginary part of the effective permittivity term, $\text{Im}(\epsilon_g)$ is

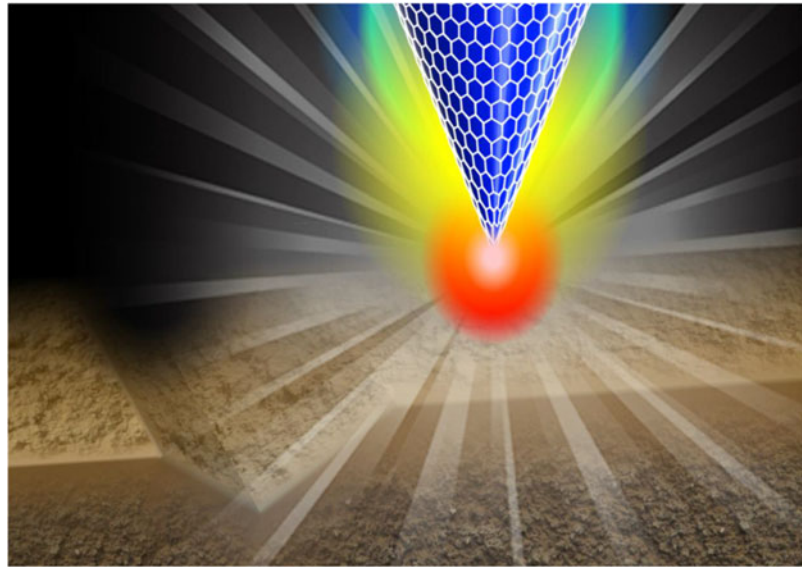


Fig. 1. Schematic of the NSOM tip coated with a layer of graphene. SPPs propagate on the lateral walls of a conical NSOM tip and are concentrated at the apex.

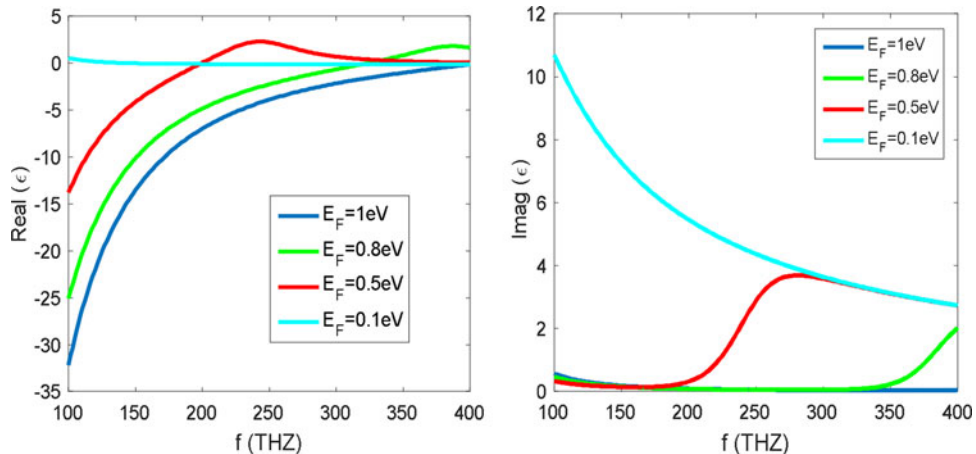


Fig. 2. Calculated graphene permittivity. (a) Real parts of graphene permittivity as a function of frequency biased at 0.1, 0.5, 0.8, and 1 eV at 100 THz ($3 \mu\text{m}$) to 400 THz (750 nm). (b) Imaginary parts of the graphene permittivity corresponding to (a).

remarkably small in a certain frequency band for high Fermi levels, showing that waves in this composite material can propagate with minimal attenuation. The Fermi levels in Fig. 2 vary from 0.1 eV (which corresponds to carrier density of $n_s = 7.33 \times 10^{11} \text{ cm}^{-2}$) to 1 eV ($n_s = 7.33 \times 10^{13} \text{ cm}^{-2}$).

For graphene to be able to support the propagation of SPPs, the permittivity condition ($\text{Re}(\epsilon_g) < -1$) must be satisfied. From Fig. 2(a) we notice that for our operating frequency range this can only be achieved for high Fermi levels (higher than 0.8 eV). A very delightful property of SPPs at this operating frequency is that for a sufficiently high Fermi level, the plasmon losses in graphene are extremely small as it can be seen from Fig. 2(b). Transverse-magnetic (TM) SPP surface waves on graphene are governed by the dispersion relation

$$\beta_g = k_0 \sqrt{1 - \left(\frac{2}{\sigma_g(\omega) n_0} \right)^2} \quad (2)$$

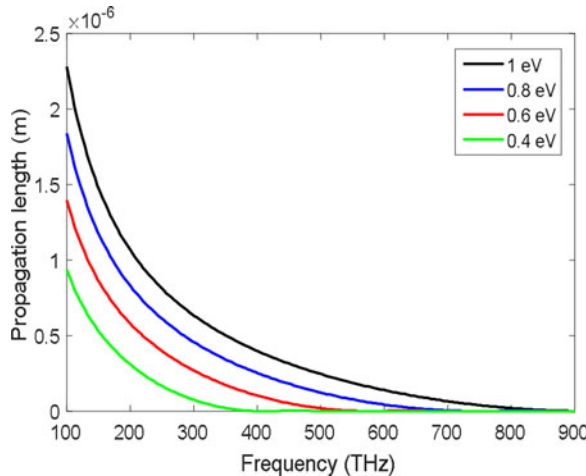


Fig. 3. Propagation length of TM SPP waves on graphene as a function of frequency for different Fermi level.

where β_g and k_0 are the wave numbers of the guided mode and the free space, respectively, and η_0 is the intrinsic impedance of free space. The propagation length can be calculated by $L_{sppg} = 1/Im(\beta_g)$. Fig. 3 presents the TM SPP wave propagation length with respect to frequency for different Fermi levels.

According to the above analysis, it can be realized that THz surface plasmon waves on graphene have the advantage of tunability which allows us to dramatically decrease the loss in the system via increasing the Fermi level. On the other hand, the propagation length is short and the plasmon waves are not strongly excited (the real part of permittivity is not negative enough compared to the permittivity of noble metals at this frequency, the larger the real part of permittivity, the stronger the amplitude of SPP excitation). In order to compensate for this problem, two important factors have been considered in this paper. First, it has been shown that graphene layer has numerous ripples (bubbles) on the surface [16], [17]. These sharp edges act as active emission sites to enhance the electron field emission. Second, the angle of excitation can play a critical role in order to excite graphene surface plasmons on the lateral walls of the designed probes. Here, the optimized angle of 83.4° has been achieved via sweeping the excitation angle through FEM analysis. Another important parameter in increasing the amplitude of SPPs, as mentioned in the above analysis is the Fermi level. In this work, it has been set to be 1 eV. A conical probe with a tip angle of $\Theta = 38.8^\circ$ is considered for both probe type A and B, which may be obtained by anisotropic wet etching process.

The calculated magnetic field intensity on the lateral surface of probe type A and type B is shown in Fig. 4. As it can be seen, the surface plasmon waves are confined to the lateral walls of the tips and are localized at the apex of the NSOM probes in both cases. Although type B has stronger confinement and higher magnetic field intensity, it requires an extra dielectric layer with $\epsilon_d = 1.35$ at 960 nm wavelength. The dielectric layer is 30 nm thick and is placed on top of the probe, between the tip and graphene layer as presented in Fig. 4(b). To evaluate the optical resolution of proposed probes, the full-width-at-half-maximum (FWHM) is defined by the distribution of the total electric field density near the probe tip as shown in our previous work [18]. FWHM analysis results, electric energy density, and the electric field density plots are presented in Fig. 5.

The calculated results are measured at 20 nm below the tip apex. It can be observed that the electrical energy density of type A is the highest (10^{13}) and has been augmented more than 10^6 times compared to a single aperture probe (with 10^7). For type B, the amplitude is one-tenth that of type A due to dielectric loss, but it exhibits lower FWHM, meaning a confinement of the near field to a smaller region. Obtained results possess a large electric field enhancement over recently reported metallic plasmonic probes [19].

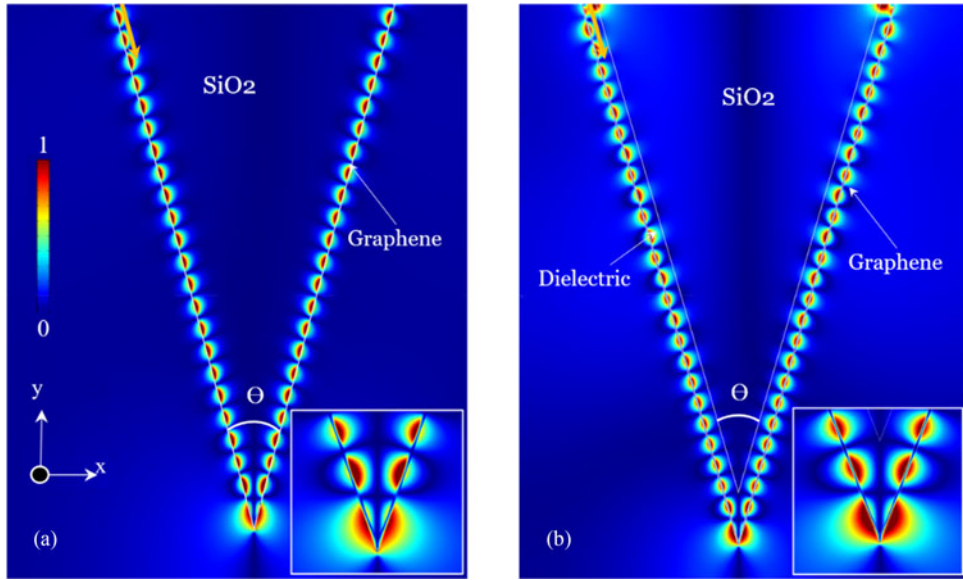


Fig. 4. Magnetic field distribution $|B_z|$. (a) Type A (just SiO_2) and (b) type B (SiO_2 tip is covered with low refractive index dielectric, $\epsilon_d = 1.3$). Orange color arrows present the TM excitation direction. The tip angle is $\Theta = 38.8^\circ$.

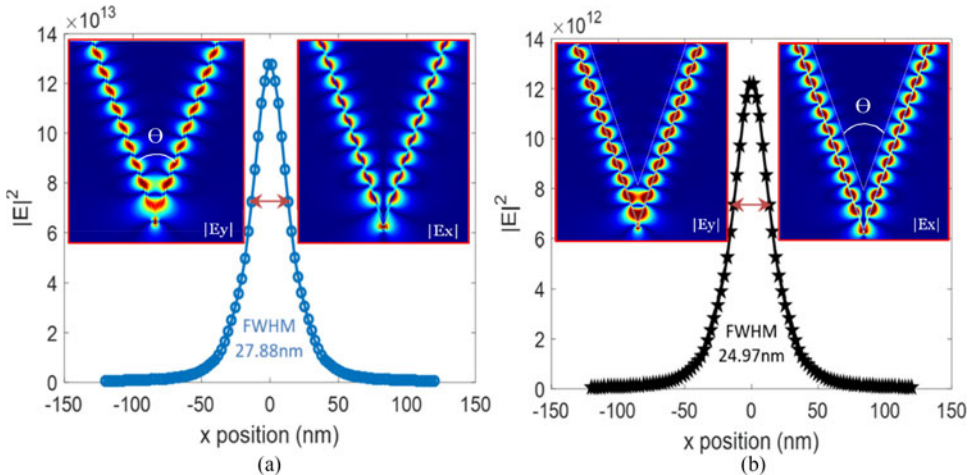


Fig. 5. FWHM and electric field distribution in y ($|E_y|$) and x ($|E_x|$) directions for the proposed probes for 20 nm tip-sample distance. (a) Type A. (b) Type B. Calculated FWHM for type B (24.97 nm) has smaller value than type A (27.88 nm), same coordinate system as in Fig. 4. ($\Theta = 38.8^\circ$).

Finally, we have analyzed the tip-sample distance effect and the frequency influence on the performance of each designed probe. In Fig. 6(a), the calculated FWHM of each probe corresponding to various tip-sample distances is shown. Within 70 nm from the probe tip, the FWHM of both probe type A and B is less than 60 nm, and the two designed probes still hold a large energy density enhancement (over three orders of magnitude compared to the simple aperture probe the aperture size of 20 nm). Below 50 nm tip-sample distance, probe type B presents smaller FWHM compared to probe type A. Fig. 6(b) shows the spectral characteristics of the two probe designs in the near-field region. It is obvious that the designed probes based on graphene are extremely sensitive to frequency variation due to frequency dependency of permittivity of graphene, which is consistent with the previous theoretical analysis in this paper.

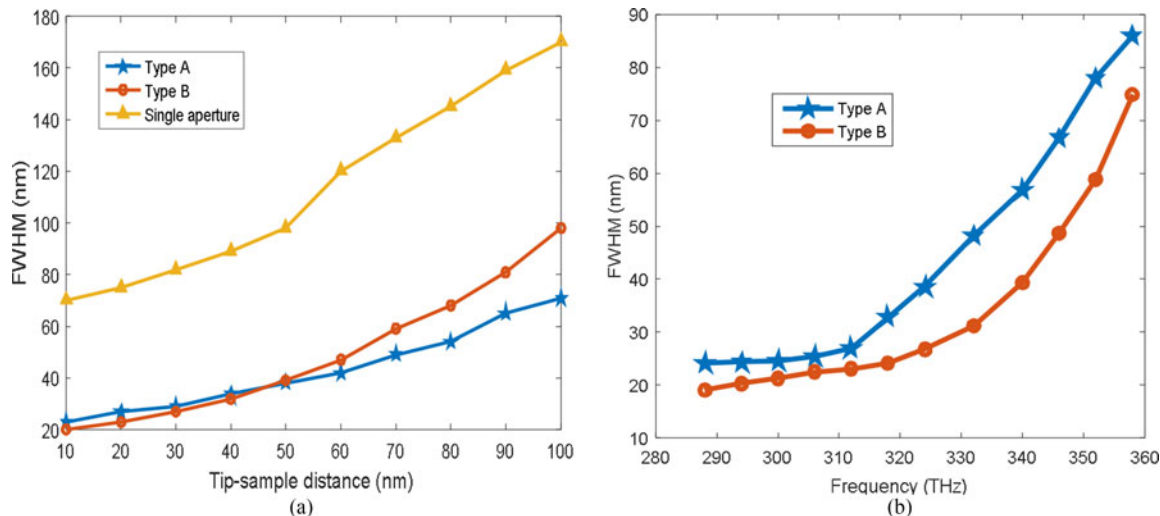


Fig. 6. Near-field characteristics of three probes. (a) Type A, type B, and classical single aperture probe (20 nm aperture size) at 312 THz. (b) Spectral characteristics of the designed probes.

3. Summary

This paper numerically investigates the propagation of surface plasmons on the surface of monolayer graphene. Based on the theoretical analysis results, we reported two NSOM probe designs with enhanced nanofocusing capabilities with graphene plasmonics mechanism. To our knowledge, this is the first example in the literature of NSOM plasmonic probes capable of exploiting graphene plasmons. In order to excite SPP waves at the operating frequency (312 THz), two critical parameters—namely the Fermi level and the excitation angle—are optimized based on the FEM solution. To benchmark the nanofocusing capabilities, the performance of the designed probes is analyzed in terms of FWHM and frequency, and compared with those of conventional single aperture and typical metallic plasmonic probes reported in the literature. Over three order of magnitude near-field enhancement is achieved via the proposed designs. The designs possess very low FWHM, about two times smaller than the silver probes, due to two-dimensionality, and high surface-to-volume ratio in graphene. Graphene plasmonics may enable novel probe design which can lead to a new generation of near-field scanning optical microscopy tailored for high spatial, spectral and temporal-resolution imaging.

Acknowledgment

The authors thank Prof. S. D. Gedney of the University of Colorado, Denver, for fruitful discussion and guidance.

References

- [1] H. Raether, *Surface Plasmons on Smooth Surfaces*. New York, NY, USA: Springer, 1988.
- [2] H. T. Chorsi, M. T. Chorsi, and X. J. Zhang, "Using graphene plasmonics to boost biosensor sensitivity," *SPIE Biomed. Opt. Med. Imag.*, 2016, doi: 10.1117/2.1201610.006712.
- [3] T. L. Vasconcelos et al., "Tuning localized surface plasmon resonance in scanning near-field optical microscopy probes," *ACS Nano*, vol. 9, no. 6, pp. 6297–6304, 2015.
- [4] H. T. Chorsi and S. D. Gedney, "Efficient high-order analysis of bowtie nanoantennas using the locally corrected Nystrom method," *Opt. Exp.*, vol. 23, no. 24, pp. 31452–31459, 2015.
- [5] M. Zekriti, D. V. Nesterenko, and Z. Sekkat, "Long-range surface plasmons supported by a bilayer metallic structure for sensing applications," *Appl. Opt.*, vol. 54, no. 8, pp. 2151–2157, 2015.
- [6] S. Kawata, "Near-field microscope probes utilizing surface plasmon polaritons," in *Near-Field Optics and Surface Plasmon Polaritons*, S. Kawata, Ed. Berlin, Germany: Springer, 2001.

- [7] X. Luo, T. Qiu, W. Lu, and Z. Ni, "Plasmons in graphene: Recent progress and applications," *Mater. Sci. Eng. R, Rep.*, vol. 74, no. 11, pp. 351–376, 2013.
- [8] K. S. A. Novoselov *et al.*, "Two-dimensional gas of massless Dirac fermions in graphene," *Nature*, vol. 438, no. 7065, pp. 197–200, 2005.
- [9] Q. Bao and K. P. Loh, "Graphene photonics, plasmonics, and broadband optoelectronic devices," *ACS Nano*, vol. 6, no. 5, pp. 3677–3694, 2012.
- [10] K. S. Novoselov *et al.*, "Electric field effect in atomically thin carbon films," *Science*, vol. 306, no. 569, pp. 666–669, 2004.
- [11] A. N. Grigorenko, M. Polini, and K. S. Novoselov, "Graphene plasmonics," *Nature Photon.*, vol. 6, no. 11, pp. 749–758, 2012.
- [12] V. P. Gusynin, S. G. Sharapov, and J. P. Carbotte, "Magneto-optical conductivity in graphene," *J. Phys., Condensed Matter*, vol. 19, no. 2, 2007, Art. no. 026222.
- [13] H. T. Chorsi and S. D. Gedney, "Tunable plasmonic optoelectronic devices based on graphene metasurfaces," *IEEE Photon. Technol. Lett.*, vol. 29, no. 2, pp. 228–230, Jan. 2016.
- [14] A. B. Kuzmenko, E. van Heumen, F. Carbone, and D. van der Marel, "Universal optical conductance of graphite," *Phys. Rev. Lett.*, vol. 100, no. 11, 2008, Art. no. 117401.
- [15] K. F. Mak, M. Y. Steir, Y. Wu, C. H. Lui, J. A. Misewich, and T. F. Heinz, "Measurement of the optical conductivity of graphene," *Phys. Rev. Lett.*, vol. 101, no. 19, 2008, Art. no. 196405.
- [16] N. Armbrust, J. Gütter, P. Jakob, and U. Höfer, "Time-resolved two-photon photoemission of unoccupied electronic states of periodically rippled graphene on Ru(0001)," *Phys. Rev. Lett.*, vol. 108, no. 5, 2012, Art. no. 056801.
- [17] Z. S. Wu *et al.*, "Field emission of single-layer graphene films prepared by electrophoretic deposition," *Adv. Mater.*, vol. 21, no. 17, pp. 1756–1760, 2009.
- [18] Y. Lee, A. Alu, and X. J. Zhang, "Efficient apertureless scanning probes using patterned plasmonic surfaces," *Opt. Exp.*, vol. 19, no. 27, pp. 25990–25999, 2011.
- [19] Y. Wang, Y.-Y. Huang, and X. J. Zhang, "Plasmonic nanograting tip design for high power throughput near-field scanning aperture probe," *Opt. Exp.*, vol. 18, no. 13, pp. 14004–14011, 2010.